UC Davis

UC Davis Previously Published Works

Title

A majority rule approach for region-of-interest-guided streamline fiber tractography

Permalink

https://escholarship.org/uc/item/8w41v37n

Journal

Brain Imaging and Behavior, 10(4)

ISSN

1931-7557

Authors

Colon-Perez, LM
Triplett, W
Bohsali, A
et al.

Publication Date

2016-12-01

DOI

10.1007/s11682-015-9474-5

Peer reviewed

eScholarship.org Powered by the California Digital Library
University of California

Author Manuscript

Author Manuscript

Author Manuscript

Author Manuscript

HHS Public Access

Author manuscript

Brain Imaging Behav. Author manuscript; available in PMC 2017 December 01.

Published in final edited form as:

Brain Imaging Behav. 2016 December ; 10(4): 1137–1147. doi:10.1007/s11682-015-9474-5.

A Majority Rule Approach for Region-of-Interest-Guided Streamline Fiber Tractography

L. Colon-Perez[a], **W. Triplett**[b], **A. Bohsali**[c], **M. Corti**[d], **P.T. Nguyen**[e], **C. Patten**[b], **T.H. Mareci**[a], and **C.C. Price**[e]

[a]Departments of Biochemistry and Molecular Biology, University of Florida, Gainesville, FL

[b]Departments of Physical Therapy, University of Florida, Gainesville, FL

[c]Veterans Affairs Brain Rehabilitation Research Center, Malcolm Randall VA Center Gainesville, FL

[d]Departments of Pediatrics, University of Florida, Gainesville, FL

[e]Departments of Clinical and Health Psychology, University of Florida, Gainesville, FL

Abstract

Objective—Hand-drawn gray matter regions of interest (ROI) are often used to guide the estimation of white matter tractography, obtained from diffusion-weighted magnetic resonance imaging (DWI), in healthy and in patient populations. However, such ROIs are vulnerable to rater bias of the individual segmenting the ROIs, scan variability, and individual differences in neuroanatomy. In this report, a “majority rule” approach is introduced for ROI segmentation used to guide streamline tractography in white matter structures.

Methods—DWI of one healthy participant was acquired in ten separate sessions using a 3T scanner over the course of a month. Four raters identified ROIs within the left hemisphere [Cerebral Peduncle (CPED); Internal Capsule (IC); Hand Portion of the Motor Cortex, or Hand Bump, (HB)] using a group-established standard operating procedure for ROI definition to guide the estimation of streamline tracts within the corticospinal tract (CST). Each rater traced the ROIs twice for each scan session. The overlap of each rater's two ROIs was used to define a representative ROI for each rater. These ROIs were combined to create a “majority rules” ROI, in which the rule requires that each voxel is selected by at least three of four raters. Reproducibility for ROIs and CST segmentations were analyzed with the Dice Similarity Coefficient (DSC).

Results—Intra-rater reliability for each ROI was high (DSCs ≥ 0.83). Inter-rater reliability was moderate to adequate (DSC range 0.54 - 0.75; lowest for IC). Using intersected majority rules ROIs, the resulting CST showed improved overlap (DSC = 0.82) in the estimated streamline tracks for the ten sessions.

Correspondence: Catherine Price, Ph.D., Associate Professor, Clinical and Health Psychology, University of Florida, Gainesville, Florida, cep23@phhp.ufl.edu; Thomas Mareci, Ph.D., Biochemistry and Molecular Biology, University of Florida, Gainesville, Florida, thmareci@ufl.edu.

Compliance with Ethical Standards: Authors Colon-Perez, L., Triplett, W., Bohsali, A., Corti, M., Nguyen, P.T., Patten, C., Mareci, T.H., and Price, C.C. declare that they have no conflict of interest. Informed consent: Written informed consent was obtained in compliance with Institutional Review Board guidelines of the University of Florida

Author Manuscript Author Manuscript Author Manuscript Author Manuscript

Conclusion—Despite high intra-rater reliability, there was lower inter-rater reliability consistent with the expectation of rater bias. Employing the majority rules method improved reliability in the overlap of the CST.

1. Introduction

White matter streamline tractography using diffusion-weighted magnetic resonance imaging (DWI) has been widely used to estimate connections between gray matter (GM) regions and the morphology of white matter structures (e.g., corticospinal tract, corpus callosum, cingulum) (Basser and Pierpaoli 1996; Jones 2010). However, tracking results depend upon the regions of interest (ROI) used to estimate white matter pathways (Cammoun et al. 2012; Jones and Pierpaoli 2005). Thus, ROI selection influences the final interpretation of white matter estimation and integrity. Most frequently, ROIs used to guide the estimation of streamline fiber tracts are defined using automated ROI segmentation templates [e.g. FreeSurfer (Fischl 2012)] or manually segmented ROIs (Kaur et al. 2014; Bucci et al. 2013). Both of these approaches have methodological shortcomings. Automated segmentation methods employing standard space templates assume a high degree of spatial agreement between individual participant's anatomy and that of the template. This assumption does not always hold, particularly for neurological patient populations. Manual segmentation of the ROIs introduces rater bias and variability even if a highly structured standard operating procedure is followed (Heye et al. 2013). Additionally, training and experience in the interpretation of a given anatomical structure may influence ROI segmentation.

The corticospinal tract (CST) is a key neuroanatomical pathway that mediates the nervous system's control of movement (Jane et al. 1968). The CST originates in well-defined cortical regions that correspond to anatomical locations throughout the body (i.e., fingers, hand, and arm). There is evidence that the CST is involved in motor coordination, movement disorders (Said et al. 2014), stroke (Kou et al. 2013; Kunimatsu et al. 2003; Lee et al. 2005; Vargas et al. 2013) and ischemia (Tang et al. 2010). Integrity of the CST (e.g., from stroke and multiple sclerosis) often results in poor motor limb control, paresis, or paralysis (Sterr et al. 2014; Zheng and Schlaug 2015). Clinical researchers are pursuing stimulation for corticospinal neurogenesis (Rosso et al. 2013; Nakagawa et al. 2013). Some have attempted to use the CST to model applications of deep brain stimulation in Parkinson's disease (Said et al. 2014), but with varying results. Therefore, there is a need to appropriately and reliably characterize the CST pathway for treatment and intervention purposes. Tractography protocols attempting to segment the CST have been performed using a two (Kunimatsu et al. 2003; Bucci et al. 2013; Lee et al. 2005; Tang et al. 2010; Vargas et al. 2013; Yasmin et al. 2009) or three ROIs (Kou et al. 2013; Min et al. 2014). Most commonly ROIs are defined within the brain stem (e.g. cerebral peduncle, and pons), internal capsule and areas of the motor cortex.

In order to understand whether observed changes to the CST are associated with pathology, manual segmentation methods must have high degree of specificity and reliability in identification and segmentation of the ROIs. To this end, we introduce the “majority rule” method for segmentation of anatomical locations used to isolate the CST. The majority rule has been described as an automatic method of pattern recognition (Kittler et al. 1998). The

Author Manuscript Author Manuscript Author Manuscript Author Manuscript

'majority rule' in our study refers to a cumulative ROI resulting from combining manually segmented ROIs from all of the raters and retaining only the portions of the ROI that were common to at least three out of the four raters. We hypothesized that combining ROIs from all raters and selecting a cumulative region common to at least three raters would reduce rater bias inherent to all manual segmentation approaches. Towards this end, four raters completed ROI segmentation to guide CST tractography. Intra rater and inter-rater measurements were acquired from one individual who was scanned on the same scanner at ten separate sessions. This unique data set allowed us to examine variations within rater without biasing them to patient differences. Additionally, this dataset allowed us to examine variations associated with different scan sessions alone.

2. Methods

2.1. Subject

We acquired structural MR imaging data from a 38 y.o., male, right-handed participant. The participant was a native English speaker with no history of neurological disorders. Written informed consent was obtained in compliance with Institutional Review Board guidelines of the University of Florida. Room temperature measurement and measurements of diffusion in a phantom ensured consistency of scanner performance at each time point.

2.2. Data Acquisition

MR data was acquired from a Siemens 3 T Verio scanner using an 8-channel head coil. High-angular resolution diffusion imaging (HARDI) data were acquired using a FOV = 23 cm × 23 cm, and TR / TE = 17300 / 81 ms. A total of 73 interleaved axial slices with a slice thickness of 2 mm were acquired. The diffusion gradients were applied along 6 directions with b = 100 s/mm^2 and 64 directions with b = 1000 s/mm^2, distributed over a sphere following a model of electrostatic repulsion (Jones et al. 1999).

DWI is sensitive to the diffusional characteristics of water molecules in isotropic and anisotropic tissue environments (Callaghan 1991). Diffusion tensor imaging (DTI) is the most commonly applied procedure for modeling diffusion properties from DWI, but has known limitations. DTI is successful in modeling diffusion in regions with strong and coherent white matter structures, such as the spinal cord, corpus callosum and cingulum, but fails in regions containing multiple fiber orientations. This limitation has prompted the development of improved methods to model diffusion in complex tissue regions, such as the Mixture of Wisharts tensor distribution [MOW (Jian et al. 2007) and Q-ball imaging (Tuch 2004), which use the enhanced acquisition techniques such as HARDI (Tuch et al. 1999).

2.3. Diffusion Data Processing

The diffusion-weighted data were first interpolated to improve spatial resolution, an approach frequently employed in tractogrpahy studies (Ford et al. 2013; Parker et al. 2003; Jellison et al. 2004; Kuceyeski et al. 2013). We used cubic convolution (Park and Schowengerdt, 1983) in all three dimensions [CONGRID function in IDL (Exelis, McLean, VA)] to interpolate the voxel dimension to 1 mm^3 isotropic resolution. For each voxel in the DWI, the diffusion displacement probability function (DPF) was estimated using a method

Author Manuscript Author Manuscript Author Manuscript Author Manuscript

of Wishart (MOW) distributions mixture of rank-2 diffusion tensors, which allows the resolution of crossing and kissing fibers (Jian et al. 2007). The largest displacement probabilities were extracted and the resulting maxima (assuming antipodal symmetry) were recorded as white matter streamline fiber orientations to be used in tractography. DTI measures of fractional anisotropy (FA) and average diffusivity (AD) maps were also calculated from the DWI data using in-house software developed in IDL. Advanced diffusion models, like MOW, have been shown to be more sensitive than DTI in segmenting the CST for intraoperative electrical stimulation (Bucci et al. 2013). Moreover, employing tractography to estimate white matter structures, like the CST, supersedes the use of atlases; FA values obtained with tractography have been found to be higher than values found when employing atlases, implying that volume averaging is reducing values along the tract (Vargas et al. 2013).

Seed points were evenly distributed on a 4^3 (64) point grid within each voxel over the whole brain; streamlines were then launched bi-directionally for all seeds (Mori and van Zijl 2002). Streamlines progressed in 0.25 mm increments along the fiber orientation of each voxel, and when encountering a voxel containing more than one possible orientation (e.g. crossing or kissing fibers), the direction most in-line with the streamline's current path of travel was selected. During tractography, streamlines tracking continued until the following stopping criteria were met: 1) the tract turned by more than 70 degrees, or 2) a low anisotropy region ($FA < 0.05$) was encountered.

2.4. Segmentation of Regions of Interest (ROIs) for the Estimating the Corticospinal Tract

In our study, the hand portion of the motor cortex, or the hand bump, was defined as the superior border of the CST, the internal capsule as a region along the CST, and the cerebral peduncle as the inferior extent of the pathway.

Four raters (ROI drawers; AB, CPr, MC, WT) met to devise, revise, and then establish a standard operating procedure (SOP) to manually segment the regions within the left hemisphere (see later section on Hand Bump, Internal Capsule and Cerebral Peduncle). Once the SOP was finalized, each of the four raters (AB, CPr, MC, WT) reviewed de-identified, randomized datasets containing the 10 DWI acquisitions. Each rater segmented the three ROIs in all 10 datasets randomly twice for a total of 20 dataset segmentations per rater. Raters kept logs to document slice locations. Problematic regions were discussed by the raters and then re-measured from re-blinded datasets by all raters. Using this procedure, each rater generated 20 ROIs per anatomical region (one per scan session and a repeat of each scan session).

Hand Bump (HB)—The HB was segmented using the FA maps. As suggested by Yousry et. al. (Yousry et al. 1997), raters recorded the slice where the brain's midline is located in a three-dimensional view, then identified the location of the sulcus that appears superior to the cingulum and continues until it reaches the precentral gyrus. Then the HB was identified visually as a “knob-like” structure located just posterior to the junction of the superior frontal sulcus with the pre-central sulcus.

Author Manuscript Author Manuscript Author Manuscript Author Manuscript

Internal Capsule (IC)—The IC was segmented on the FA maps. Raters recorded the axial slice where the most superior part of the internal capsule could be identified. This was located where the external capsule and the posterior limb of the internal capsule could be clearly identified, generally immediately underneath the fornix. The most inferior axial slice, which was one slice above the anterior commissure, was then recorded. Segmentation began at the midpoint between these slices and included one inferior and one superior slice (for a total of three slices).

Cerebral Peduncle (CPED)—The CPED was segmented on the orientation FA maps (scales by the primary eigenvector). Raters recorded the axial slice number where the inferior portion of the corticospinal tract could be identified and the slice immediately below the axial slice where the peduncular “ears” could not be distinguished from the surrounding white matter. The midpoint between these two slices was identified (roughly near the upper surface of the pons). This location served as a starting point for the segmentation of the CPED. Raters outlined ROIs on the five superior and inferior slices relative to this midpoint.

2.5. Registration Template

By visual inspection, a reference dataset (one of the ten acquisitions) with minimal rotation in any of the axial, sagittal, or coronal views, served as the image registration reference. Each of the datasets was registered to this reference using 9-degrees of freedom using FMRIB's Linear Image Registration Tool (FLIRT; (Jenkinson and Smith 2001); http://fsl.fmrib.ox.ac.uk/fsl/flirt). These registered data sets were then averaged together to produce an image-template to define the ROIs to guide tract estimation in a standard space specific to the ten data sets used in this study.

2.6 ROI Segmentation (Figure 1)

As described below, two ROIs were derived from the manual segmentations: 1) a rater representative ROI for each rater, and 2) a “Majority Rules” ROI. These ROIs are used to examine the reliability of these segmentation schemes.

2.6.1. Rater-representative ROI—Each rater's manually segmented ROI was registered to the template FA map described in the “Registration Template” section (note that all ROIs from this point forward are registered unless otherwise specified). The rater representative ROI was obtained from the intersection of the rater's two manual segmentations of the same scan session for each of the three ROIs. This resulted in four sets (one for each rater) of rater-representative ROIs per scan session for each anatomical region (HB, IC, CPED).

2.6.2. Majority Rules ROI—For each anatomical region, all four rater-representative ROIs were combined to generate a majority rules ROI for each scan session. In order to include a voxel as a member of the majority rules ROI, the voxel must have been included in at least three of the four rater-representative ROIs.

2.7. Corticospinal Tract Streamline Fibers

The CST was estimated from the relevant streamlines that connected the HB and CPED while passing through the IC for each scanning session. The HB and CPED served as

Author Manuscript Author Manuscript Author Manuscript Author Manuscript

termination ROIs, while the IC served as an intermediate (or waypoint) ROI. No additional exclusion or guiding ROIs were used in the filtering process. To estimate the CST, a fiber density map was generated, consisting of a three-dimensional volume where each voxel's value represented the number of streamlines passing through the voxel. To eliminate the contribution from spurious streamlines, only voxels with a value above a threshold of 1% of the maximum density were retained in the fiber density maps. Finally the three-dimensional volume of the CST was calculated as the number of voxels × voxel volume using the estimated CST connecting the HB and CPED ROIs.

2.8. Reproducibility Analysis and comparisons

The Dice similarity coefficient (DSC) and coefficient of variation (C_v) were used to compare the reproducibility of the ROIs and estimated CST streamline fibers. The DSC is a statistical measure of the spatial overlap of two distinct groups. It has a range between 0 and 1, with 0 indicating no overlap and 1 indicating perfect agreement between groups. Obtaining a DSC value greater than 0.7 indicates an excellent agreement between two raters (Zijdenbos et al. 1994a). The C_v is calculated as the ratio of the measurement standard deviation divided by its mean and multiplied by 100 to provide an intuitive estimate of variance expressed as a relative percentage. The ROIs were tested for reproducibility with three different comparison schemes:

1. *Intra-rater / Intra-session* (comparison of rater against self): Comparisons between the two manual segmentations of each ROI in the same scan acquisition by the same rater. This yielded 10 comparisons for each rater per ROI (3) yielding a total of 30 comparisons per rater.
2. *Intra-rater / Inter-session* (Comparison of rater between sessions): Comparisons of each rater-representative ROI from each scan session to all others scan sessions, 45 per ROI [(session 1 vs session 2, 1 vs 3, … or 10 scans × 9 comparisons) / 2] for a total of 135 comparisons per rater.
3. *Inter-rater / Intra-session* (Comparison of raters within sessions): Comparisons of the rater-representative ROI between raters for the same scan session. This yields 60 comparisons [(10 sessions, rater 1 vs rater 2, 1 vs 3, …, or 4 raters × 3 comparisons) / 2] resulting in 180 comparisons per rater for the 3 ROI's.

Given an expected increased variance between scan sessions and the individual rater's ability to hand-segment ROIs, we expected highest overlap in intra rater/intra session and lowest overlap in inter-rater / inter-session.

Tractography reproducibility was assessed with two different comparison schemes:

1. *Intra-rater / Intra-session*: Comparison of CST tract volume obtained with each rater's manual ROI segmentation of each ROI for each session for a total of 30 comparisons.
2. *Each rater-representative ROI vs. the majority rules / intra-session*: Comparison of CST tract volume obtained with each rater-representative

Author Manuscript Author Manuscript Author Manuscript Author Manuscript

ROI segmentation to the majority rules ROI for each session for a total of 30 comparisons.

The estimated CST also allows the calculation of FA and AD values along the CST path, and tractography derived measures: 1) edge weight (Hagmann et al. 2007), 2) tract count, 3) tract length, and 4) axial tract cross-sectional area. The edge weight, $w(e)$ of edge e and is defined as

$$w(e)=\frac{2}{S_i+S_{jfE_j}}\frac{1}{l(f)}, \quad (1)$$

where S_i is the surface of the connecting nodes, f is a streamline that connects the nodes, E_f is set of all streamlines connecting the nodes, and $l(f)$, is the length of streamline f. The edge weight includes all streamlines connecting the nodes regardless of their location of origin. The track count is the number of streamlines defining the CST, track average cross-sectional is the average area of the CST in axial slices, and track length is the average length of the streamline fibers in the estimated CST.

3. Results

3.1. Region-of-Interest Reproducibility

3.1.1. Intra-rater / Intra-session (Table 1, Figure 2A)—The mean DSC ranged from 0.83 to 0.87 for all raters and ROIs. Manual ROI segmentation was the most variable for the IC (DSC = 0.83, C_v = 14%) and the most consistent for the HB (DSC = 0.83, C_v = 6.0%). Therefore manual segmentation by each rater for a particular session was very consistent (i.e. DCS > 0.7).

3.1.2. Intra-rater / Inter-session (Table 1, Figure 2B)—The mean DSC for the rater-representative ROIs between sessions ranged from 0.67 to 0.80, indicating that rater manual ROI segmentation was more variable between scanning sessions than in the same session, with the most variability in IC segmentation (DSC = 0.67; C_v = 22%). A comparison of the Intra-rater/Intra-session to Intra-rater/Inter-session shows that the HB and CPED mean overlap (DSC) values displayed a percentage change of 4.8% and 8.0% on average, respectively; while the IC showed a percentage change of 19.3%. Individual rater results (Figure 2B) show that all but one rater (R2) had increased variability in IC segmentation. The percentage change for all ROI DSCs was less in the intra-rater/intra-session than the intra-rater / inter-session (percentage of change: HB = 4.8%; IC = 19.3%; CPED = 8.0%).

3.1.3. Inter-rater / Intra-session (Table 1, Figure 2C)—The range in mean DSC is the broadest (0.54 to 0.75) and has the lowest average, with the most variability in the segmentation of the IC. The IC was consistently the least reproducible segmentation across all raters, which suggests that the IC ROI is not well defined.

Author Manuscript Author Manuscript Author Manuscript Author Manuscript

3.2. Tractography reproducibility

Figure 3 shows the estimated CSTs derived using the rater-representative ROIs to filter the streamline tracts before and after thresholding with a 1% fiber density maximum (Figure 3A and 3C). Employing a 1% thresholding to maintain streamlines connecting ROIs reduced the contribution of spurious streamlines linking the ROIs. The streamlines are represented as an ROI by assigning a voxel containing the streamlines to be a voxel in the CST ROI (Fig. 3B and 3D).

Intra-rater / Intra session (Figure 4): Raters' intra-session ROI sets produced reliable CST segmentation for each imaging session. The mean DSCs for each rater (n=10 imaging sessions) were R1: 0.82 ± 0.10, R2: 0.87 ± 0.08, R3: 0.95 ± 0.03, R4: 0.94 ± 0.03 (Fig. 4a). There were differences between raters (Figure 4): Raters 3 and 4 were more reliable than raters 1 and 2, which displayed greater variability.

Rater representative specific versus Majority Rules ROI (Figure 5): individual raters DSC values were adequate to excellent (R1: 0.72 ± 0.20, R2: 0.83 ± 0.11, R3: 0.93 ± 0.03, R4: 0.94 ± 0.03. Employing the Majority rule ROI set, the mean DSC computed at 1% fiber density threshold across the 10 imaging sessions was 0.61 ± 0.03 (range: 0.57 - 0.64). The distribution of the DSC values is shown in Figure 5a.

Track volumes measured for each session using the majority rules ROIs are shown in Figure 5B. The mean track volume was 1102 ± 261 mm^3 (range: 851.5 – 1580.3 mm^3). The axial tract cross sectional area (CSA) was calculated along the path of the streamlines. Fig. 5C shows the average CSA along the path for the majority rules ROI. The values in CSA range from 8.7 mm^2 to 20.3 mm^2 with an average of 13.5 mm^2. Three tractography results for the “majority rules” ROIs are displayed in Figure 6. A parallel additional pathway can be observed in imaging session 8 resulting in a larger cross sectional area than imaging sessions 1 and 6.

CST segmentation statistics for the majority rules pathway (Table 2) were highly consistent (2.60% and 2.85% coefficient of variation.) The average edge weight was 295.75 ± 192.35, the track count was 24360.0 ± 15662.5, and the average length of the streamlines for all sessions was found to be 82.8 ± 1.6. Rater specific segmentation of the CST displayed similar variations across all raters (Table 3). The average streamline length displayed very good reliability, but the edge weight displayed higher variation across all raters.

4. Discussion

4.1. Main Findings

The present study investigated variability of ROI segmentation by expert raters and its effects on tractography and diffusion metrics. At least three important points were identified: 1) as expected, intra-rater was higher than inter-rater reliability due to variability between certain raters; 2) the internal capsule had the lowest intra- and inter-rater reliability due to difficulty in defining the anatomy from the slices; and 3) despite variations in inter-rater reliability and segmentation difficulty with the internal capsule, employment of a majority rules approach resulted in highly consistent CST segmentation across the ten scans. These

Author Manuscript Author Manuscript Author Manuscript Author Manuscript

collective findings suggest that a majority rule approach to ROI segmentation is one viable option for improving fiber modeling using DWI approaches. The combination of the manually delineated ROIs created by multiple raters (i.e. majority rules) helps ameliorate rater bias, which often times can lead to problems quantifying structural networks derived from DWI and tractography.

4.2. Region of interest reliability

The comparison between template and CST tracts has been assessed (Vargas et al. 2013), showing that both techniques show similar correlations with behavioral analysis. However, the tractography approach shows increased FA values compared to the atlas-segmented CSTs. The lower FA values in the atlas approach can be attributed to volume averaging of voxels that do not correspond to the CST; therefore, we did not employ the atlas approach.

Despite adequate training and standardized operating procedures, each rater showed variability in manual segmentation of ROIs. This was evident even when raters were compared on measurements from the same scan (intra rater / intra session). Reliability was reduced even further (4% to 19% decline in regional segmentation overlap) when the regions of interest were compared across multiple scan sessions (Intra rater/ Inter session or test retest). This is striking because all raters were measuring the same individual across all scan sessions; therefore rater variability in the test-retest is independent of subject variability. The observed variability is most likely influenced by the subject head alignments in the MR scanner for any particular day. Test-retest reliability ranged from 0.67 to 0.80, which indicates reasonable variability between raters (Table 1). The worst raters show a reliability of 0.66 for the HB, 0.68 CPED, and 0.17 for the IC. The 0.17 indicates that one rater had difficulty identifying the IC between scans, which is similar variability displayed in manually segmented tumors (Warfield et al. 2006). All comparisons concur that IC displayed the least reproducibility, particularly in the test-retest reliability (intra rater/inter session). The test-retest is particularly difficult for this ROI since only the middle portion of the IC was used as a control region to define the path or tract and reduce the number of spurious streamlines. This variability is due to inconsistent choices of starting slices combined with the small number (3) of slices making up the IC ROI in this study. Raters did not select the same initial and final slice. If a rater began their ROI one slice above or one slice below another rater, then at least one third of the ROI will be different. Of note, the HB and CPED regions of interest displayed acceptable reproducibility (DSC > 0.74) relative to suggested dice coefficient guidelines (Zijdenbos et al. 1994b).

Reliability dropped further when different raters were compared within the same session (Inter-rater/ intra-session); 10 to 35% more variable than the same rater within the same scan session (intra-rater/ intra-session). Although inter-rater scores are expected to be lower than intra-rater scores [e.g., (Kaur et al. 2014)], we do note that the range we observed was quite large. This range is attributed to discrepancy in the segmentation of one particular region of interest the internal capsule.

Author Manuscript Author Manuscript Author Manuscript Author Manuscript

4.3. Corticospinal tract segmentation from tractography

The majority rule ROI combined elements of all raters' segmentations thereby requiring that the final ROI involve overlap from at least three of the four raters. Each rater's segmented CST (intra-rater / inter-session) relative to the majority rules segmented CST had moderate overlap. Given that there is currently no ‘gold standard’ for ROI definition unless strongly based upon cytoarchitectural definitions or gross anatomical landmarks [e.g., (Insausti et al. 1998)], our data suggest that having multiple rater views is essential in order to reduce rater bias for the CST. For our study, the CST, the majority rules ROI yielded a final reproducibility index (DSC) greater than 0.57 with a 3.2% coefficient of variation across all sessions. We consider this more than acceptable given the following argument.

The CST studied here (i.e. the portion connecting to HB) can be considered analogous to a cylinder, whereby its volume involves length and cross sectional area. Any variability in the measurement of the cylinder will relate to its longitudinal or cross sectional area variation. For our study, the average CST length using the majority rule ROIs varied only about 2%. The cross sectional area (Fig 5C), however, displayed more variability with an average area of 13.5 mm^2 and the variation along the track of 28.7%. The main source of variability shown in Fig 5C is due the external streamlines that make up the path as shown in Fig 6. Therefore the variability of the total CST volumes (23.7%) shown in Fig 5B is most likely related directly to the variability in cross sectional area and extraneous streamlines at the edge of the bulk of the CST pathway. Previous studies have shown that error accumulates as track lengths increase (Miles and Laidlaw 2012). Since the portion of the CST examined in this study has a path length around 6 times larger than the width of its cross sectional area, it is not unreasonable to fail to achieve excellent DSC values (> 0.85), given the difficulty associated with replicating a “long” and “skinny” track such as the CST with MR images acquired at 2 mm isotropic resolution. Therefore our result of DSC's around 0.60 represents an acceptable level of variation in CST segmentation; given the track length and the difficulty in segmenting the ROI's that define the track of this fiber path. Visual inspection of the tracks showed great similarity in the CST's obtained in this study.

4.3 Limitations

The CST length was in the range of 80mm, and error accumulation in tractography is directly related to the tract length. We recognize that diffusion spectrum imaging (DSI) is considered a superior model for tractography studies for pathways in the range of 50 – 100mm (Gigandet et al. 2013). DSI, however, requires additional acquisition times and cost. We employed HARDI as the data acquisition method and MOW to reconstruct fiber orientations; these two served as a compromise to estimate crossing fibers and have reasonable scan times. For the current study, we wanted to examine the reliability of structure assessment using diffusion-weighted approaches that are currently being acquired clinically and applied to surgery populations of interest. We also recognize a potential limitation with the type of ROI selected. The HB and IC ROIs in this study are small and the image resolution (2mm isotropic) limited. Even with linear interpolation in the DWI images, we recognize there may be other approaches for modeling WM from DWIs (Yap and Shen 2012; Yap et al. 2014). In this study we only made use of a ten scans of a single subject, so it is not our desire to claim perfect CST segmentations rather present a possible method to

Author Manuscript Author Manuscript Author Manuscript Author Manuscript

define ROIs for tractography in populations where the use of atlases is difficult and not warranted. Despite these limitations, we propose that our a priori study design addressed a problematic area within the field of tractography, since we assessed the same individual over time and employed a standardized operating procedure to assess rater measurement of regions of interest in cortex, brainstem, and white matter regions. Additionally, we propose a majority rule approach in order to improve a well-known problem of intra-rater drift across scan sessions, but also inter-rater variance within and between sessions. Finally, we sought to improve the modeling of a clinically relevant fiber structure – the CST.

4.4. Future directions and applicability in future studies

Manual segmentation is the preferred method for delineating regions of interest in heterogeneous populations, such as those with dementia or stroke. In the current study, our majority rules ROI consisted of voxels contained in ROIs defined by any three out of the four raters within gray matter. We recognize this approach is not always feasible, particularly in clinical practice and the use of the majority rules approach will depend on availability of trained raters. Therefore we encourage further research on integrating rater-based majority rules regions of interest with machine learning algorithms. A promising option to guide machine learning is in the use of the STAPLE method (Warfield et al. 2004, 2006). This method seeks to generate an estimate of the ground truth from a set of segmented trials. Those segmentations can be manual (as the ones presented in this article), generated by algorithmic raters (e.g. Freesurfer) or a combination of both. In populations that algorithmic raters might not be accurate the majority rules ROIs can be generated with combination of algorithm and human raters. Hence estimates of the “real” segmentation could be generated that would not have the rater bias of human raters or the homogeneity of algorithmic raters.

5. Conclusion

In this study, we present an approach for the segmentation of anatomical structures useful for the determination of white matter tracts and assessed the reproducibility of CST segmentation from a single subject scanned (i.e. with HARDI acquisition) in multiple sessions. The reproducibility of the CST obtained with manual segmentation did not result in the highly reproducible values; however, the CST showed satisfactory reproducibility when a “majority rule” scheme was employed to define the anatomical ROIs. This study suggests the feasibility of tracking the CST without the need of atlases. The next step may be to apply the majority rule approach to a dataset that assesses structure-function relationships, and to address the feasibility of using the majority rule approach to ROI segmentation in machine-based algorithms.

Acknowledgments

The authors would like to acknowledge Sam Crowley for his reviews of the manuscript draft. Funding was provided by NIH grants K23 NS060660, RO1 NR014181, and R01 NS082386, as well as the UF Center for Movement Disorder and Neurorestoration and the Brain and Spinal Cord Injury Research Trust Fund of the State of Florida. A portion of this work was performed in the University of Florida McKnight Brain Institute at the National High Magnetic Field Laboratory's AMRIS Facility, which is supported by National Science Foundation Cooperative Agreement No. DMR-1157490, the State of Florida, and the U.S. Department of Energy.

Author Manuscript Author Manuscript Author Manuscript Author Manuscript

Study Funding/ Disclosures - Supported by NINDS K23NS60660; NINDS R01 NS082386; NINR R01 NR014181; University of Florida Center for Movement Disorders and Neurorestoration

References

Basser PJ, Pierpaoli C. Microstructural and Physiological Features of Tissues Elucidated by Quantitative-Diffusion-Tensor MRI. Journal of Magnetic Resonance, Series B. 1996; 111(3):209–219. doi:http://dx.doi.org/10.1006/jmrb.1996.0086. [PubMed: 8661285]

Bucci M, Mandelli ML, Berman JI, Amirbekian B, Nguyen C, Berger MS, Henry RG. Quantifying diffusion MRI tractography of the corticospinal tract in brain tumors with deterministic and probabilistic methods. Neuroimage Clin. 2013; 3:361–368. DOI: 10.1016/j.nicl.2013.08.008 [PubMed: 24273719]

Callaghan, P. Principles of Nuclear Magnetic Resonance Microscopy. Oxford University Press; Oxford, England: 1991.

Cammoun L, Gigandet X, Meskaldji D, Thiran JP, Sporns O, Do KQ, Maeder P, Meuli R, Hagmann P. Mapping the human connectome at multiple scales with diffusion spectrum MRI. Journal of neuroscience methods. 2012; 203(2):386–397. DOI: 10.1016/j.jneumeth.2011.09.031 [PubMed: 22001222]

Fischl B. FreeSurfer. NeuroImage. 2012; 62(2):774–781. DOI: 10.1016/j.neuroimage.2012.01.021 [PubMed: 22248573]

Ford A, Triplett W, Sudhyadhom A, Gullett J, McGregor K, FitzGerald D, Mareci T, White K, Crosson B. Broca's Area and Its Striatal and Thalamic Connections: A Diffusion-MRI Tractography Study. Frontiers in Neuroanatomy. 2013; 7doi: 10.3389/fnana.2013.00008

Gigandet X, Griffa A, Kober T, Daducci A, Gilbert G, Connelly A, Hagmann P, Meuli R, Thiran JP, Krueger G. A connectome-based comparison of diffusion MRI schemes. PLoS One. 2013; 8(9):e75061.doi: 10.1371/journal.pone.0075061 [PubMed: 24073235]

Hagmann P, Kurant M, Gigandet X, Thiran P, Wedeen VJ, Meuli R, Thiran JP. Mapping human whole-brain structural networks with diffusion MRI. PLoS ONE. 2007; 2(7):e597. [PubMed: 17611629]

Heye T, Merkle EM, Reiner CS, Davenport MS, Horvath JJ, Feuerlein S, Breault SR, Gall P, Bashir MR, Dale BM, Kiraly AP, Boll DT. Reproducibility of dynamic contrast-enhanced MR imaging. Part II. Comparison of intra- and interobserver variability with manual region of interest placement versus semiautomatic lesion segmentation and histogram analysis. Radiology. 2013; 266(3):812–821. DOI: 10.1148/radiol.12120255 [PubMed: 23220891]

Insausti R, Juottonen K, Soininen H, Insausti A, Partanen K, Vainio P, Laakso M, Pitkanen A. MR volumetric analysis of the human entorhinal, perirhinal, and temporopolar cortices. American Journal of Neuroradiology. 1998; 19(4):659–671. [PubMed: 9576651]

Jane JA, Yashon D, Becker DP, Beatty R, Sugar O. The effect of destruction of the corticospinal tract in the human cerebral peduncle upon motor function and involuntary movements. Report of 11 cases. J Neurosurg. 1968; 29(6):581–585. DOI: 10.3171/jns.1968.29.6.0581 [PubMed: 4237130]

Jellison BJ, Field AS, Medow J, Lazar M, Salamat MS, Alexander AL. Diffusion tensor imaging of cerebral white matter: a pictorial review of physics, fiber tract anatomy, and tumor imaging patterns. AJNR Am J Neuroradiol. 2004; 25(3):356–369. [PubMed: 15037456]

Jenkinson M, Smith S. A global optimisation method for robust affine registration of brain images. Medical image analysis. 2001; 5(2):143–156. [PubMed: 11516708]

Jian B, Vemuri BC, Ozarslan E, Carney PR, Mareci TH. A novel tensor distribution model for the diffusion-weighted MR signal. Neuroimage. 2007; 37(1):164–176. doi:S1053-8119(07)00273-X[pii]10.1016/j.neuroimage.2007.03.074. [PubMed: 17570683]

Jones, DK., editor. Diffusion MRI: Theory, Methods, and Applications. Oxford University Press; New York, NY: 2010.

Jones DK, Horsfield MA, Simmons A. Optimal strategies for measuring diffusion in anisotropic systems by magnetic resonance imaging. Magn Reson Med. 1999; 42(3):515–525. [PubMed: 10467296]

Author Manuscript Author Manuscript Author Manuscript Author Manuscript

Jones DK, Pierpaoli C. Confidence mapping in diffusion tensor magnetic resonance imaging tractography using a bootstrap approach. Magn Reson Med. 2005; 53(5):1143–1149. DOI: 10.1002/mrm.20466 [PubMed: 15844149]

Kaur S, Powell S, He L, Pierson CR, Parikh NA. Reliability and repeatability of quantitative tractography methods for mapping structural white matter connectivity in preterm and term infants at term-equivalent age. PLoS One. 2014; 9(1):e85807.doi: 10.1371/journal.pone.0085807 [PubMed: 24475054]

Kikinis R, Shenton ME, Gerig G, Martin J, Anderson M, Metcalf D, Guttmann CR, McCarley RW, Lorensen W, Cline H, et al. Routine quantitative analysis of brain and cerebrospinal fluid spaces with MR imaging. J Magn Reson Imaging. 1992; 2(6):619–629. [PubMed: 1446105]

Kittler J, Hatef M, Duin RPW, Matas J. On Combining Classifiers. IEEE Transactions On Pattern Analysis and Machine Intelligence. 1998; 20(3):14.

Kou N, Park CH, Seghier ML, Leff AP, Ward NS. Can fully automated detection of corticospinal tract damage be used in stroke patients? Neurology. 2013; 80(24):2242–2245. DOI: 10.1212/WNL.0b013e318296e977 [PubMed: 23658388]

Kuceyeski A, Meyerhoff DJ, Durazzo TC, Raj A. Loss in connectivity among regions of the brain reward system in alcohol dependence. Hum Brain Mapp. 2013; 34(12):3129–3142. DOI: 10.1002/hbm.22132 [PubMed: 22815206]

Kunimatsu A, Aoki S, Masutani Y, Abe O, Mori H, Ohtomo K. Three-dimensional white matter tractography by diffusion tensor imaging in ischaemic stroke involving the corticospinal tract. Neuroradiology. 2003; 45(8):532–535. DOI: 10.1007/s00234-003-0974-4 [PubMed: 12856090]

Lee JS, Han MK, Kim SH, Kwon OK, Kim JH. Fiber tracking by diffusion tensor imaging in corticospinal tract stroke: Topographical correlation with clinical symptoms. Neuroimage. 2005; 26(3):771–776. DOI: 10.1016/j.neuroimage.2005.02.036 [PubMed: 15955486]

Miles, J.; Laidlaw, DH. Predicting DTI Tractography Uncertainty from Diffusion-Weighted-Image Noise; ISMRM 20th Annual Meeting & Exhibition; Melbourne, Australia. 2012. p. 19062012

Min ZG, Rana N, Niu C, Ji HM, Zhang M. Does diffusion tensor tractography of the corticospinal tract correctly reflect motor function? Med Princ Pract. 2014; 23(2):174–176. DOI: 10.1159/000353463 [PubMed: 23949557]

Mori S, van Zijl PC. Fiber tracking: principles and strategies - a technical review. NMR Biomed. 2002; 15(7-8):468–480. [PubMed: 12489096]

Nakagawa H, Ueno M, Itokazu T, Yamashita T. Bilateral movement training promotes axonal remodeling of the corticospinal tract and recovery of motor function following traumatic brain injury in mice. Cell death & disease. 2013; 4:e534.doi: 10.1038/cddis.2013.62 [PubMed: 23470541]

Parker GJ, Haroon HA, Wheeler-Kingshott CA. A framework for a streamline-based probabilistic index of connectivity (PICo) using a structural interpretation of MRI diffusion measurements. J Magn Reson Imaging. 2003; 18(2):242–254. DOI: 10.1002/jmri.10350 [PubMed: 12884338]

Rosso C, Valabregue R, Attal Y, Vargas P, Gaudron M, Baronnet F, Bertasi E, Humbert F, Peskine A, Perlbarg V, Benali H, Lehericy S, Samson Y. Contribution of corticospinal tract and functional connectivity in hand motor impairment after stroke. PloS one. 2013; 8(9):e73164.doi: 10.1371/journal.pone.0073164 [PubMed: 24086272]

Said N, Elias WJ, Raghavan P, Cupino A, Tustison N, Frysinger R, Patrie J, Xin W, Wintermark M. Correlation of diffusion tensor tractography and intraoperative macrostimulation during deep brain stimulation for Parkinson disease. Journal of neurosurgery. 2014; :1–7. DOI: 10.3171/2014.6.JNS131673

Sterr A, Dean PJ, Szameitat AJ, Conforto AB, Shen S. Corticospinal tract integrity and lesion volume play different roles in chronic hemiparesis and its improvement through motor practice. Neurorehabil Neural Repair. 2014; 28(4):335–343. DOI: 10.1177/1545968313510972 [PubMed: 24334657]

Tang PF, Ko YH, Luo ZA, Yeh FC, Chen SH, Tseng WY. Tract-specific and region of interest analysis of corticospinal tract integrity in subcortical ischemic stroke: reliability and correlation with motor function of affected lower extremity. AJNR Am J Neuroradiol. 2010; 31(6):1023–1030. DOI: 10.3174/ajnr.A1981 [PubMed: 20110374]

Author Manuscript Author Manuscript Author Manuscript Author Manuscript

Tuch DS. Q-ball imaging. Magn Reson Med. 2004; 52(6):1358–1372. [PubMed: 15562495]

Tuch, DS.; Weisskoff, RM.; Belliveau, JW.; Wedeen, VJ. HIgh angular resolution diffusion imaging of the human brain Paper presented at the 7th annual meeting of the. Society for Magnetic Resonance in Medicine; Philadelphia: 1999.

Vargas P, Gaudron M, Valabregue R, Bertasi E, Humbert F, Lehericy S, Samson Y, Rosso C. Assessment of corticospinal tract (CST) damage in acute stroke patients: comparison of tract-specific analysis versus segmentation of a CST template. J Magn Reson Imaging. 2013; 37(4): 836–845. DOI: 10.1002/jmri.23870 [PubMed: 23086724]

Warfield S, Dengler J, Zaers J, Guttmann CR, Wells WM 3rd, Ettinger GJ, Hiller J, Kikinis R. Automatic identification of gray matter structures from MRI to improve the segmentation of white matter lesions. J Image Guid Surg. 1995; 1(6):326–338. DOI: 10.1002/(sici)1522-712×(1995)1:6<326::aid-igs4>3.0.co;2-c [PubMed: 9080353]

Warfield SK, Zou KH, Wells WM. Simultaneous truth and performance level estimation (STAPLE): an algorithm for the validation of image segmentation. IEEE Trans Med Imaging. 2004; 23(7):903–921. DOI: 10.1109/tmi.2004.828354 [PubMed: 15250643]

Warfield SK, Zou KH, Wells WM. Validation of image segmentation by estimating rater bias and variance. Med Image Comput Comput Assist Interv. 2006; 9(Pt 2):839–847. [PubMed: 17354851]

Yap PT, An H, Chen Y, Shen D. Fiber-driven resolution enhancement of diffusion-weighted images. NeuroImage. 2014; 84:939–950. DOI: 10.1016/j.neuroimage.2013.09.016 [PubMed: 24060317]

Yap PT, Shen D. Resolution enhancement of diffusion-weighted images by local fiber profiling. Med Image Comput Comput Assist Interv. 2012; 15(Pt 3):18–25. [PubMed: 23286109]

Yasmin H, Aoki S, Abe O, Nakata Y, Hayashi N, Masutani Y, Goto M, Ohtomo K. Tract-specific analysis of white matter pathways in healthy subjects: a pilot study using diffusion tensor MRI. Neuroradiology. 2009; 51(12):831–840. DOI: 10.1007/s00234-009-0580-1 [PubMed: 19662389]

Yousry TA, Schmid UD, Alkadhi H, Schmidt D, Peraud A, Buettner A, Winkler P. Localization of the motor hand area to a knob on the precentral gyrus. A new landmark. Brain. 1997; 120(Pt 1):141–157. [PubMed: 9055804]

Zheng X, Schlaug G. Structural white matter changes in descending motor tracts correlate with improvements in motor impairment after undergoing a treatment course of tDCS and physical therapy. Front Hum Neurosci. 2015; 9:229.doi: 10.3389/fnhum.2015.00229 [PubMed: 25983684]

Zijdenbos AP, Dawant BM, Margolin RA, Palmer AC. Morphometric analysis of white matter lesions in MR images: method and validation. IEEE Trans Med Imaging. 1994a; 13(4):716–724. DOI: 10.1109/42.363096 [PubMed: 18218550]

Zijdenbos AP, Dawant BM, Margolin RA, Palmer AC. Morphometric analysis of white matter lesions in MR images: method and validation. IEEE transactions on medical imaging. 1994b; 13(4):716–724. DOI: 10.1109/42.363096 [PubMed: 18218550]

Author Manuscript Author Manuscript Author Manuscript Author Manuscript

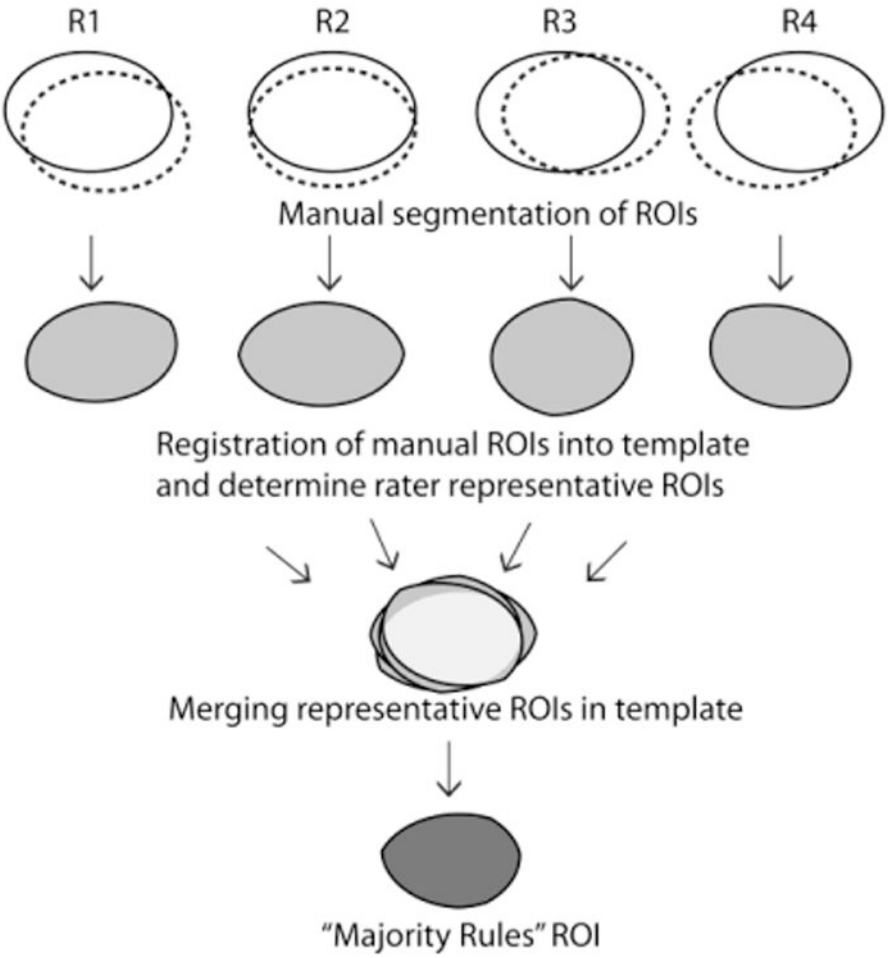

Figure 1.

Flow diagram of region-of-interest (ROI) generation for a single scan session. First, each rater created two manual segmentations of the same ROI for each scan session. Second, image data from each scanning sessions was registered to a common template (see text). Third, the intersection of the two manually segmented ROI generated a rater-representative ROI for each scan session. Finally voxels common to at least three raters were used to generate the "Majority Rules" ROI.

Author Manuscript Author Manuscript Author Manuscript Author Manuscript

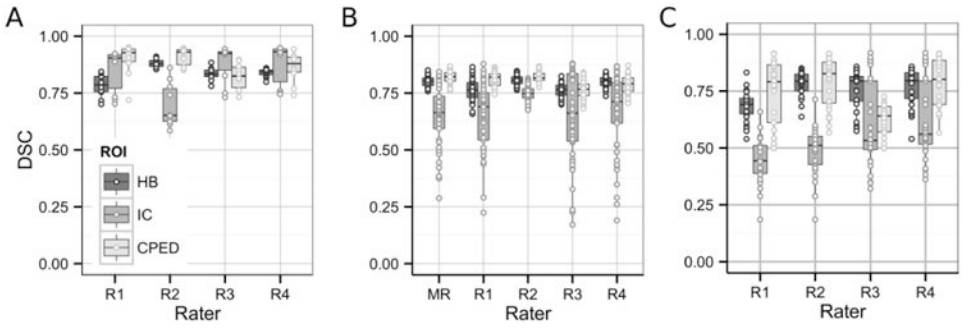

Figure 2.

Dice similarity coefficient (DSC) results for the 3 regions of interest (ROI); hand bump (HB), cerebral peduncle (CPED) and internal capsule (IC)). (A) Intra-rater/ Intra-session DSC boxplots for each rater's ROIs. ROIs were compared between their first and second attempt for each of the 10 imaging sessions. (B) Intra-rater / Inter-session DSC boxplots for each rater-representative ROI (intersection of attempt 1 vs attempt 2) and majority rules (MR) ROI. ROI's were compared for each of the 10 imaging trials. (C) Inter-rater / Intra-session DSC boxplots rater-representative ROI. ROI's were compared for each of the 10 imaging trials.

Author Manuscript Author Manuscript Author Manuscript Author Manuscript

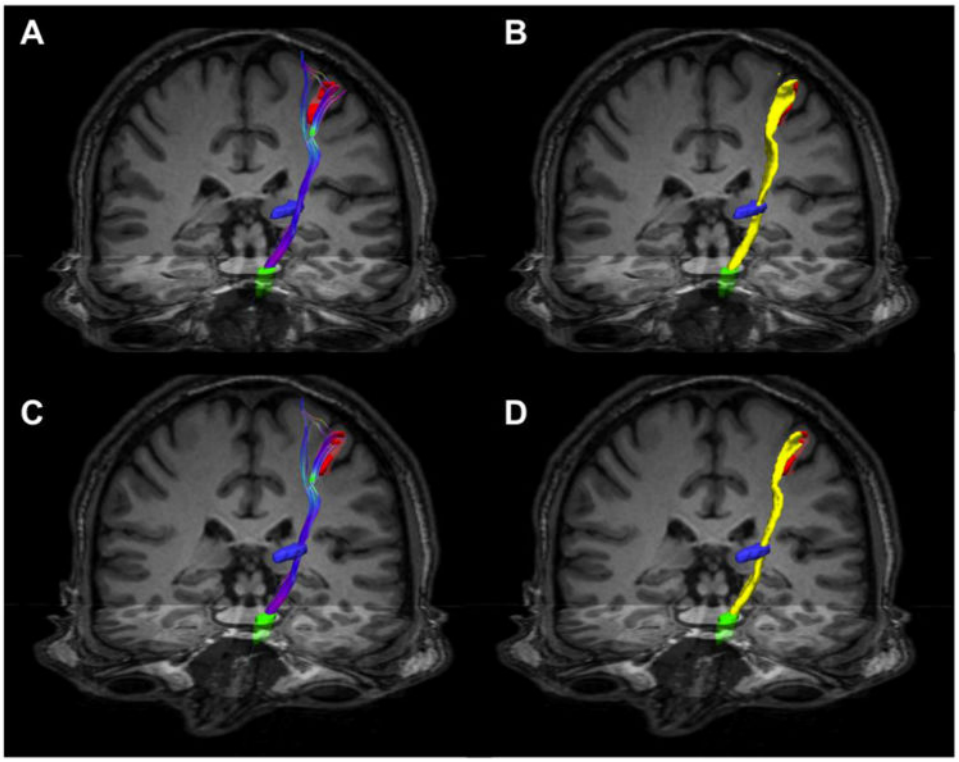

Figure 3.

Estimated streamlines of the corticospinal tract (CST) using the rater-representative hand bump (HB), internal capsule (IC) and cerebral penduncle (CPED) ROIs as filters to define the CST. (A & C) Resulting streamlines after filtering procedure for different imaging sessions and same subject. (B & D) Estimated CST (in yellow) after thresholding to remove streamline fibers less that 1% of maximum fiber count for each imaging session. In all panels, the PED, IC, and HB are displayed in green, blue, and red color respectively.

Author Manuscript Author Manuscript Author Manuscript Author Manuscript

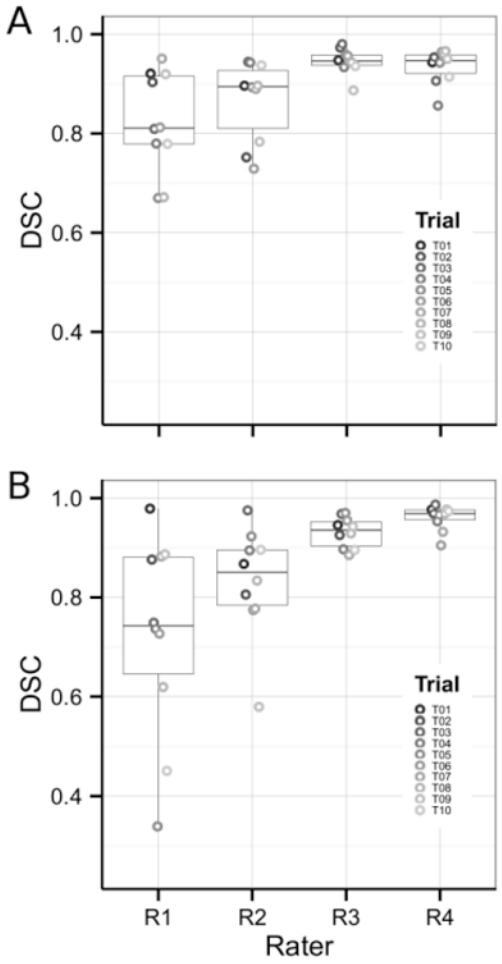

Figure 4.

Comparison of estimated corticospinal tract. Box and jitter plots shows the distribution of Dice similarity coefficient (DSC) values for each rater over the 10 imaging session. (A) Intra-rater, intra-session tractography results, and (B) Inter-rater, intra-session tractography results.

Author Manuscript Author Manuscript Author Manuscript Author Manuscript

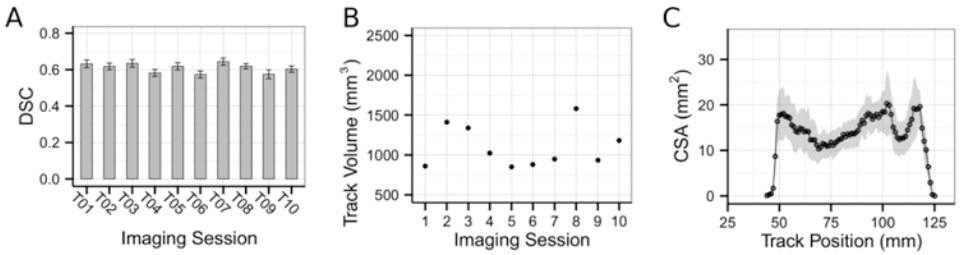

Figure 5.

Cortico-spinal tract statistics (A) Dice similarity coefficient (DSC) tractography results of cortico-spinal tract (Intra-rater / Inter-session) segmentation, showing the mean ± standard deviation of DSC values. (B) Inter-session tract segmentation volumes using the majority-rules ROI set. Visit-count maps were thresholded at 1% of max visit count before converting to binary segmentations. (C) Tract cross-sectional area (CSA) of the majority-rules ROI set's tractography traversing inferior to superior, average track CSA with standard deviations indicated as shaded regions. Visit counts thresholded at 1% of max visit count.

Author Manuscript Author Manuscript Author Manuscript Author Manuscript

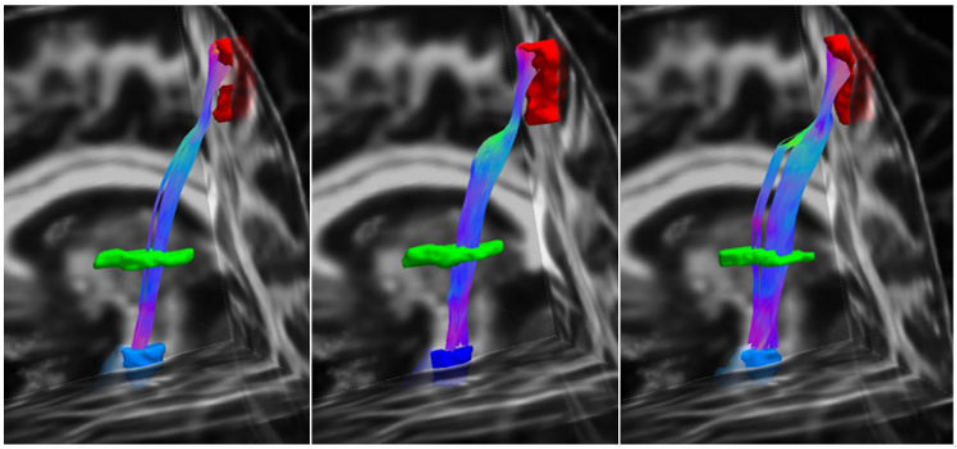

Figure 6.

Representative images of variability seen in Figure 4C. Obtained streamlines connecting the "majority rules" ROI resulting of imaging sessions 1 (left), 6 (center), and 8 (right).

Author Manuscript Author Manuscript Author Manuscript Author Manuscript

Table 1

Mean Dice similarity coefficient (DSC) for hand bump (HB), internal capsule (IC) and cerebral peduncle (CPED).

	Mean DSC	σ DSC	C_v (%)	Min DSC	Max DSC	Median DSC
Intra-rater / Intra-session						
HB	0.83	0.05	6.0	0.70	0.91	0.84
IC	0.83	0.12	14	0.59	0.95	0.89
CPED	0.87	0.07	8.0	0.72	0.95	0.89
Intra-rater / Inter-session						
HB	0.79	0.04	5.1	0.66	0.86	0.79
IC	0.67	0.15	22	0.17	0.88	0.71
CPED	0.80	0.04	5.0	0.68	0.87	0.81
Inter-rater / Intra-session						
HB	0.75	0.08	11	0.54	0.86	0.78
IC	0.54	0.16	30	0.19	0.92	0.52
CPED	0.74	0.13	18	0.50	0.92	0.74

*Mean DSC = mean across all raters and all sessions. σ DSC = is the standard deviation, C_V = is the coefficient of variation (σ/mean).

Author Manuscript Author Manuscript Author Manuscript Author Manuscript

Table 2

Diffusion and tractography in the corticospinal tract (CST) based on “majority rules” region of interest markers*.

Imaging Session	DSC	FA	AD (×10^{-4} mm^2/s)	Volume (mm^3)	Edge Weight (mm^{-3})	Average Length (mm)	Track Count
1	0.63 ± 0.04	0.30 ± 0.30	3.63 ± 3.75	861.25	132.49	80.60	10675
2	0.62 ± 0.05	0.32 ± 0.31	3.60 ± 3.39	1414.75	593.79	80.05	47463
3	0.63 ± 0.05	0.30 ± 0.30	3.70 ± 3.58	1340.50	423.90	84.62	35835
4	0.58 ± 0.04	0.31 ± 0.31	3.56 ± 3.37	1024.50	336.75	83.24	28000
5	0.62 ± 0.05	0.30 ± 0.30	3.70 ± 3.64	851.50	117.99	84.68	9987
6	0.57 ± 0.05	0.30 ± 0.30	3.71 ± 3.64	881.00	145.24	84.31	12228
7	0.64 ± 0.04	0.31 ± 0.30	3.64 ± 3.43	950.75	193.90	81.66	15811
8	0.62 ± 0.05	0.31 ± 0.29	3.83 ± 3.52	1580.25	593.21	82.60	48943
9	0.57 ± 0.05	0.29 ± 0.29	3.86 ± 3.82	935.00	84.34	83.49	7038
10	0.60 ± 0.05	0.31 ± 0.29	3.85 ± 3.57	1180.25	335.93	82.31	27620

*Streamline fibers included in the CST were thresholded at 1% of maximum fiber count; DSC = Dice Similarity Coefficient; Fractional anisotropy (FA) and average diffusivity (AD) are computed as averages over the entire CST. Volume is calculated for the thresholded CST. Edge Weight is computed as in Hagmann et al (ref).

Author Manuscript Author Manuscript Author Manuscript Author Manuscript

Table 3

Rater specific corticospinal tract (CST) parameters derived from tractography where each rater's representative ROI was used to determine the edge weight, track count and average path length of the CST tract.

	Edge Weight (mm^{-3})	σ	C_v (%)	Average Length (mm)	σ	C_v (%)	Track Count	σ	C_v (%)
R1	150.0	109.9	73.27	82.9	0.97	1.17	12370	8995	72.72
R2	198.1	128.2	64.72	83.2	1.33	1.60	16371	10419	63.64
R3	230.5	133.3	57.83	83.4	1.58	1.90	19200	10975	57.16
R4	171.8	103.3	60.13	84.4	1.23	1.46	14503	8707	60.03